J. Chem. Sci. Vol. 129, No. 12, December 2017, pp. 1829–1841.
https://doi.org/10.1007/s12039-017-1392-1

REGULAR ARTICLE

Fluorescent vinyl and styryl coumarins: A comprehensive DFT study of structural, electronic and NLO properties

KIRAN AVHAD, AMOL JADHAV and NAGAIYAN SEKAR*
Department of Dyestuff Technology, Institute of Chemical Technology, Matunga, Mumbai, Maharashtra 400 019, India
E-mail: n.sekar@ictmumbai.edu.in; nethi.sekar@gmail.com

MS received 30 July 2017; revised 18 September 2017; accepted 22 September 2017; published online 14 November 2017

Abstract. Nonlinear optical properties of 3-styryl and 3-vinyl coumarin dyes have been investigated with Density Functional Theory (DFT) using global hybrid (GH) and range-separated hybrid (RSH) functionals. The performance of GHs - B3LYP, BHHLYP, PBE0, M06, M06L, M062X, and M06HF and RSHs - CAM-B3LYP, HISSbPBE, HSEH1PBE, wB97, wB97X, and wB97XD in combination with 6-311++G(d,p) basis set has been analyzed. Estimated (hyper) polarizability (α_0, β_0) obtained from the GHs - M06, M062X and PBE0 are in agreement with each other. The RSHs - wB97 and wB97X estimate very close values of β_0. The β_0 value of 3-styryl and 3-vinyl coumarins reaches the maximum as the bond length alternation and bond order alternation parameters tend to zero. Natural bond orbital analysis shows there is extensive charge transfer in the excited state leading to large value of β_0. The vibrational contribution to α_0 and β_0 is significantly less when the donor is methoxy group and acceptor is nitro group in the 3-styryl coumarin. The dye, (E)-7-(diethylamino)-3-(4-nitrostyryl)-2H-chromen-2-one (**3c**) is found to give the highest NLO response. An increasing electrophilicity originating from the decreased HOMO-LUMO band gap leads to an increase in α_0 and β_0 in all the cases.

Keywords. BLA/BOA; coumarin vinyls and styryls; DFT; GHs and RSHs; nonlinear optical properties.

1. Introduction

Organic molecules with nonlinear optical (NLO) properties have wide range of applications because of their small dielectric constants,[1] electro-optical (EO) modulation characteristics,[2] ultrafast responses,[3] high optical damage thresholds, simple methods of preparation and low fabrication costs.[4–7] The π-π∗ transitions in organic molecules make them better candidates as NLO materials for wide bandwidth optoelectronic telecommunication systems in electronic/photonic integrated circuits, phased array radars, and in terahertz (THz) and spectroscopy applications.[8,9] Unlike geometric perturbations of central metal ion occurring in the crystalline inorganic NLO materials the electronic charge transfer across the organic molecules plays a key role[10,11] allowing the optical response of NLO-active organic compounds much faster over the inorganic compounds. In this context, the higher second and third order NLO properties of simple organic molecular materials have been extensively studied.[12–15]

Past few decades have witnessed developments in terms of synthesis of a huge number of organic π conjugated molecules with suitable molecular design strategies for better NLO materials.[16] Many of these molecules bear donor and acceptor groups separated by a conjugated bridge (D-π-A) with a push-pull type of arrangement.[17–22] NLO materials with good thermal and photostabilities are of great importance in photonics.[23–26] Coumarin dyes are known for their outstanding charge mobility from donor to acceptor and therefore they have been studied for their NLO properties.[27–33] Recently, pentaammineruthenium complex of coumarins 510 and 523 have been shown to have large hyperpolarizability values.[32,34] Linear and NLO properties of substituted coumarins have been recently studied experimentally[32,35] as well as using DFT computations.[36,37] Thus, theoretical computations should

*For correspondence

Electronic supplementary material: The online version of this article (https://doi.org/10.1007/s12039-017-1392-1) contains supplementary material, which is available to authorized users.

be able to throw light on the structure-property relationship of NLOphoric molecules, particularly the coumarin dyes. In the design of π conjugated polymers and molecular NLO active materials, bond length alternation (BLA) is shown to be one of the important geometrical parameters.[38–40] It has been shown that the trends in NLO properties obtained from electric field induced second harmonic generation (EFISHG) can be correlated with the BLA based on the geometry obtained from X-ray crystallographic studies[41,42] in comparison with the computational studies.[1,3,40,43,44]

In this paper, a benchmarking study has been done to understand the performance of hybrid functionals (GHs) as against range-separated hybrid functionals (RSHs) in computing the total polarizability (α_0) and static first-order hyperpolarizability (β_0) values of the coumarin dyes. The BLA, BOA parameter at ground state (GS) and excited state (ES) and β_0 values were computed from geometry optimized at B3LYP/6-311++G(d,p) level of theory. Also, a correlation is established between BLA and BOA parameters and hyperpolarizability (β_0) values of 3-styryl and 3-vinyl coumarins. The charge transfer (CT) characteristics of these molecules have been established using natural bond orbital (NBO) analysis and molecular electrostatic potential (MEP) analysis using the same level of theory. The vibrational contribution to the α_0 and β_0 values have been computed for the three series of coumarin derivatives namely **1a** to **1c**, **2a** to **2c** and **3a** to **3c** in their ground state. The present study will possibly facilitate the design of new compounds with large magnitude linear and NLO response in organic materials.

2. Computational details

Density Functional Theory (DFT) computations[45] were carried out with Gaussian 09 suit program.[46] The GH functional B3LYP which uses Becke's three parameters (local, non-local) hybrid exchange functional with Lee–Yang–Parr correlation functional[47–49] along with triple zeta basis set 6-311++G(d,p)[50] was used for optimizing the ground state geometry. Time Dependent Density Functional Theory (TD-DFT)[51] was used for obtaining vertical excitation (including triplet state) using the functionals B3LYP and CAM-B3LYP with the geometry as obtained above. DFT and TD-DFT computations in solvent environments were carried out using PCM model as implemented in Gaussian 09.[52] The B3LYP/6-311++G(d,p) optimized geometry was used to populate NBOs and to construct the MEP plots. The total polarizability and static first order hyperpolarizability values were obtained using finite field approach[53] as implemented in Gaussian 09 using both GHs and RSHs. The GHs used for polar computations are B3LYP, BHHLYP, PBE0, M06, M06L, M062X, and M06HF while the RSHs used are CAM-B3LYP, HISSbPBE, HSEH1PBE, wB9, wB97X, and wB97XD. In earlier benchmarking studies, RSH functionals have been found to perform much better than GHs for nonlinear optical properties based on comparison with highly accurate coupled-cluster models.[54–64]

Table 1. Global hybrid (GHs) and range separated hybrid (RSHs) functionals with their HF % exchange composition.

Global hybrids (GHs)		Rang separated hybrids (RSHs)	
Functional	HF %	Functional	HF %
M06L	0	HISSbPBE	-
B3LYP	20	wB97	0
PBE0	25	wB97X	15
M06	27	HSEH1PBE	25–0
BHHLYP	50	CAM-B3LYP	19–65
M06-2X	54	wB97X-D	22–100
M06-HF	100	-	-

The purpose of this work is the first instance to critically compare the performance of GHs versus RSHs in the computation of total polarizability (α_0) and the static first order hyperpolarizability (β_0) of vinyl and styryl coumarins in the light of the fact that RSHs outperform.[65,67,68] The GHs and RSHs used in the study with their best HF % exchange composition are presented in Table 1.

The components of hyperpolarizability are defined as the coefficients in the Taylor series expansion of the energy in the external electric field. When the external electric field is weak and homogeneous, Taylor series expansion of the energy becomes Eq. 1.

$$E = E^0 - \mu_1 F_1 - \frac{1}{2}\alpha_{ij} F_i F_j - \frac{1}{6}\beta_{ijk} F_i F_j F_k + \frac{1}{24}\gamma_{ijkl} F_i F_j F_k F_l + \cdots \quad (1)$$

where, E^0 is the energy of the unperturbed molecules, μ is the vector component of the dipole moment, α is the linear polarizability, F_i is the field at the origin, μ_i, α_{ij}, b_{ijk} and c_{ijkl} are respectively the components of dipole moment, polarizability, the first hyperpolarizabilities and the second hyperpolarizabilities. The total static dipole moment (μ), mean polarizability (α_0), anisotropy of polarizability ($\Delta\alpha$) and static total first order hyperpolarizability (β_0) can be calculated using the x, y and z components as:[69]

$$\mu = \left(\mu_x^2 + \mu_y^2 + \mu_z^2\right)^{\frac{1}{2}} \quad (2)$$

$$\alpha_0 = \left(\frac{1}{3}\right)\left[\alpha_{xx} + \alpha_{yy} + \alpha_{zz}\right] \quad (3)$$

$$\Delta\alpha = 2^{-\frac{1}{2}}[(\alpha_{xx} - \alpha_{yy})^2 + (\alpha_{yy} - \alpha_{zz})^2 + (\alpha_{zz} - \alpha_{xx})^2 + 6\alpha_{xx}^2]^{\frac{1}{2}} \quad (4)$$

$$\beta_{total} = \left[\left(\beta_{xxx} + \beta_{xyy} + \beta_{xzz}\right)^2 + \left(\beta_{yxx} + \beta_{yyy} + \beta_{yzz}\right)^2 + \left(\beta_{zxx} + \beta_{zyy} + \beta_{zzz}\right)^2\right]^{\frac{1}{2}} \quad (5)$$

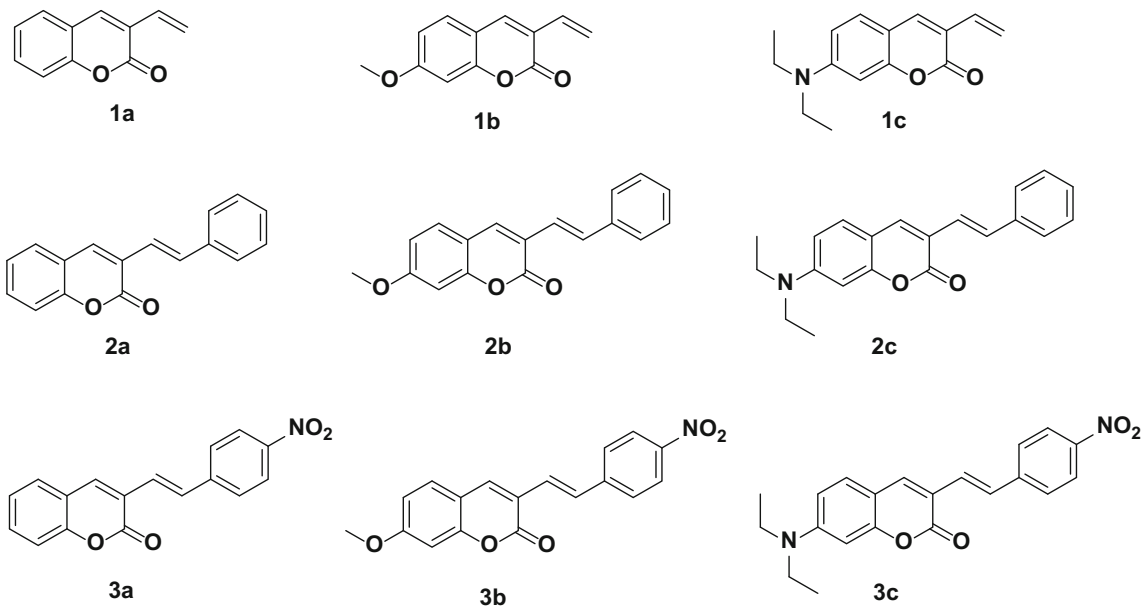

Figure 1. Structures of vinyl and styryl coumarins.

The values of total static dipole moment (μ), the mean polarizability (α_0) and the mean static total first order hyperpolarizability (β_0) of the dyes **1a**-**1c**, **2a**-**2c** and **3a**-**3c** (Figure 1) calculated in gas and acetonitrile solvent using Equations (2-5) respectively with the GHs and range RSHs using 6-311++G(d,p) basis sets. The CT parameters are defined as the delocalization energy E(2) and describe the interactions between donors (i) and acceptor (j). They are given by,

$$E\,(2) = q_i \frac{F\,(i,\,j)^2}{\varepsilon_j - \varepsilon_i} \tag{6}$$

Where, q_i is the occupation number of the donor orbital, ε_i and ε_j are diagonal elements and equal to the orbital energies. Finally, F (i, j) is the off-diagonal (off) of the Fock matrix.

In addition, we also studied the HOMO–LUMO energy band gap, global hardness η, Global softness S, Electrophilicity index ω, and energy of the intercrossing system (ΔE_{ISC}).

3. Results and Discussion

3.1 *Geometries in ground state (S_0) and lowest lying excited singlet (S_1)*

The dyes **1a**-**1c**, **2a**-**2c** and **3a**-**3c** were optimized in their ground (S_0) and lowest lying singlet excited (S_1) states with the help of DFT and TD-DFT using B3LYP/6-311++G(d,p) in the gas phase and acetonitrile environment. For illustration, the results of optimized geometry parameters of the dyes **1a**-**1c**, **2a**-**2c** and **3a**-**3c** in acetonitrile are presented in Table S1. The dyes are found to be perfectly planar in S_0 and S_1 state revealing the effective ICT character (Figure 2). NLO response in D-π-A system is well understood by molecular geometry parameter of BLA/BOA. BLA and BOA of the conjugated chain were calculated as reported.[70] Optimized structure of **3c** (Figure 2) shows that major single bond length gets shortened for the bonds N_{30}-C_{11}, C_{10}-C_8, C_3-C_4, C_5-C_{15}, C_{18}-C_{20}, C_{22}-C_{25}, C_{27}-N_{47}, the values are respectively 0.009, 0.005, 0.004, 0.013, 0.008, 0.002, 0.031 Å. The incremental lengthenings in double bonds C_{10}-C_{11}, C_8-C_3, C_4-C_5, C_{15}-C_{18}, C_{20}-C_{22}, C_{25}-C_{27} as compared to the S_0 state are respectively 0.005, 0.007, 0.010, 0.015, 0.005, 0.010 Å. Therefore the shortening and lengthening in between σ and π bonds are observed due to their partial overlap of π bond character in the donor-acceptor system. Similar results are observed for the other dyes, **1a**-**1c**, **2a**-**2c**, and **3a**-**3b.** The values are presented in Table S2a, S2b, and S2c. The BLA values for all the dyes are positive and tend to be zero, which indicate that the molecular structure is approaching towards cyanine limit (BLA = 0) from polyene limit (BLA ∼0.4–0.6). The BOA values of coumarin dyes are negative and tend to be zero, suggesting that the molecular structure is approaching towards cyanine limit (BOA = 0) from polyene limit (BOA = ∼ 0.6). Further, the values of BLA and BOA in S_0 state are more than in S_1 state which signifies that S_1 state is more polarized than S_0 state. This increase in polarization in the first excited state is responsible for the lowering of HOMO-LUMO energy gap. BLA and BOA results indicate that the dyes show more cyanine character which is desirable for enhanced NLO response.

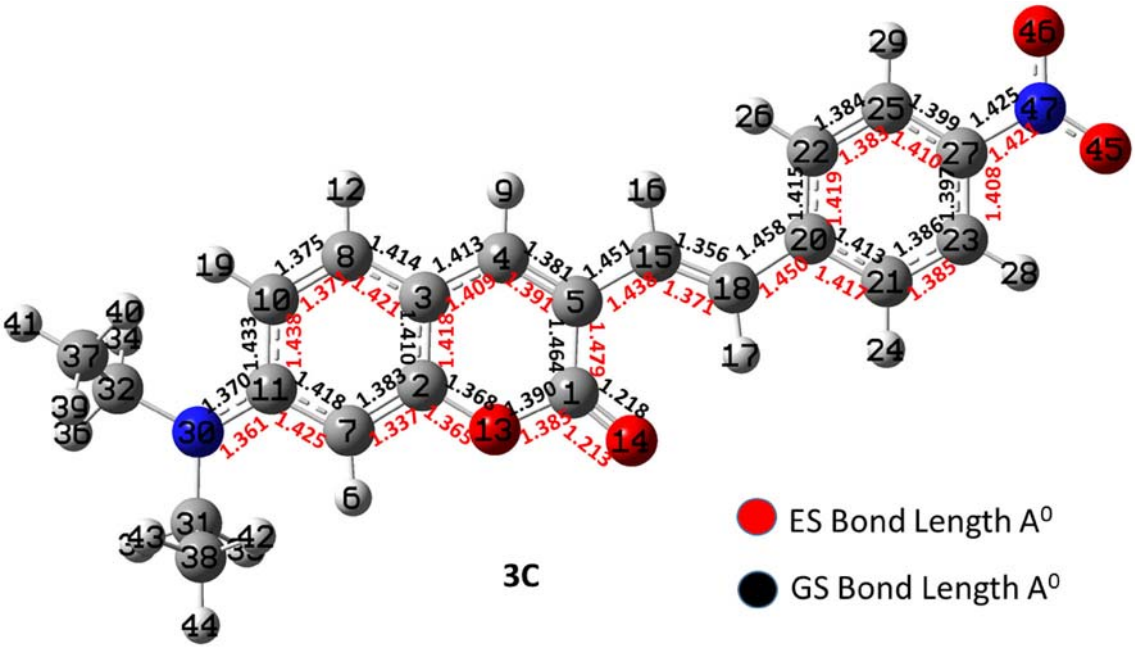

Figure 2. Optimized geometry of **3c** in acetonitrile medium at B3LYP/6-311++G(d,p) level of theory.

Table 2. Optical data of dyes **1a**-**1c**, **2a**-**2c** and **3a**-**3c**, [a]vertical excitation (nm), [b]oscillator strength and [c]experimental absorption (nm) data in the gas phase and solvent acetonitrile.

Dye	Phase	B3LYP/6-311++G(d,p)			CAM-B3LYP/6-311++G(d,p)			Exp. λ_{max}(nm)[c]
		λ_{max}(nm) [a]	f^b	OC (%) H→L	λ_{max}(nm)[a]	f^b	OC (%) H→L	
1a	Gas	323	0.437	87.73	302	0.522	90.98	326
	ACNE	329	0.598	94.12	308	0.677	94.08	
1b	Gas	333	0.692	82.05	311	0.710	94.25	333
	ACNE	346	0.761	97.58	323	0.851	96.07	
1c	Gas	365	0.731	97.16	335	0.844	95.44	400
	ACNE	392	0.844	98.31	359	0.984	96.15	
2a	Gas	377	0.952	98.27	340	1.128	95.27	351
	ACNE	388	1.066	99.03	347	1.270	95.24	
2b	Gas	381	1.080	98.65	346	3.584	95.67	366
	ACNE	394	1.218	99.23	356	1.368	95.70	
2c	Gas	403	1.294	98.87	364	1.418	95.47	421
	ACNE	428	1.419	99.23	386	1.542	95.36	
3a	Gas	401	1.122	98.28	350	1.382	92.37	371
	ACNE	447	1.102	99.56	374	1.521	88.35	
3b	Gas	422	1.116	98.79	362	1.488	88.79	392
	ACNE	481	1.075	99.70	390	1.621	83.32	
3c	Gas	468	1.101	99.27	405	1.621	77.28	459
	ACNE	566	1.029	99.99	431	1.811	75.90	

3.2 *Vertical Excitation*

The values of vertical excitation obtained from TD-B3LYP/6-311++G(d,p) and TD- CAM-B3LYP/6-311 ++G(d,p), the oscillator strengths (f) and experimental absorption (λ_{max})[71] data of dyes (**1a-1c, 2a-2c** and **3a-3c**) are summarized in Table 2. The presence of donor group at 7 positions and acceptor at 3 positions gives red-shifted absorption was found in the trends in the computed vertical excitation values. The dyes **1a-1c, 2a-2c**, and **3a-3c** have shown absorption between 320 nm and 459 nm and vertical excitation in the range of 323 nm to 566 nm and 302 nm to 431 nm using B3LYP and CAM-B3LYP functionals respectively. Among these two functionals, B3LYP shows reasonably accurate results of absorption for dyes **1a**, **1b**, **1c** and **2c** while

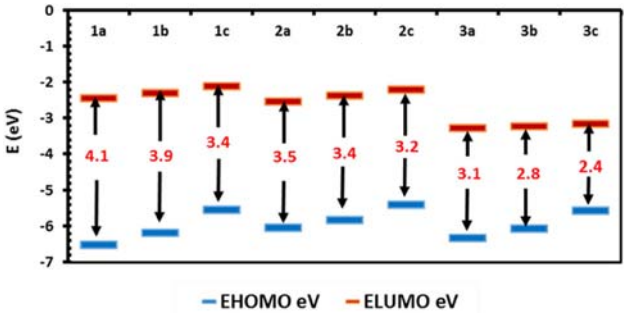

Figure 3. HOMO-LUMO energy level diagram (eV) of dyes **1a**-**1c**, **2a**-**2c** and **3a**-**3c** in acetonitrile solvent considered at the B3LYP/6-311++G(d,p) level.

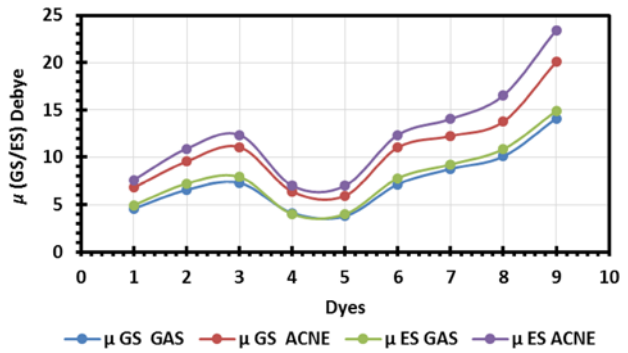

Figure 4. Dipole moment (μ in Debye) graph in the ground state (S_0) and excited state (S_1) in gas and solvent acetonitrile (ACNE) phase.

overestimates the absorption for dyes **2a**, **2b**, **3a**, **3b**, and **3c**. The values obtained using RSH, CAM-B3LYP functional are reasonably accurate with lower discrepancy as compared to the B3LYP functional. In the $-NO_2$ group containing dyes donor strength increases in the order -H <-OCH_3 <-$N(CH_2CH_3)_2$ explaining trends in red-shifted absorption as well as lowering HOMO-LUMO energy gap (Figure 3).

3.3 *Dipole moment (μ) at ground state (S_0) and excited state (S_1)*

The dipole moments of S_0 and S_1geometries were obtained from DFT and TD-DFT computations using the functional B3LYP and the basis set 6-311++G(d,p). The results are summarized in Table S3. The plots of μ of S_0 state geometries against the μ of S_1 state geometry of all the dyes are shown in Figure 4. It is evident that the trends are almost similar in all the cases. As the length of π-conjugation between donor and acceptor (**3c**) increases the μ of S_1 state increases, which shows that the S_1 state is more polar than S_0 state. Higher the value of μ more is the effective charge transfer from N, N-diethylamine donor moiety to the acceptor $-NO_2$ which in this kind of molecules is further confirmed by the distribution of electron density at HOMO and LUMO. Moreover, an increase in the ratio, μ_e/μ_g is also accompanied by a decrease in HOMO-LUMO gap leading to a red shift in emission as well as effective charge transfer. The static μ values computed using GHs and RSHs (Table S4) reveal the same trend. In case of **3c** having both NO_2 and dimethylamino group in conjugation, the highest μ was observed. As expected the donor strength increases in the order of -H < -OCH_3 <-$N(CH_2CH_3)_2$ in the dyes **1a-1c** < **2a-2c** < **3a-3c**. The ratios of dipole moment between S_0 and S_1 states suggest that the dyes are more polar in the S_1 state (Table S3).

3.4 *Charge Transfer Characteristics*

3.4a *Frontier molecular orbitals (FMOs) approach*: Frontier molecular orbital (FMOs) analysis helps in understanding the nature of intramolecular charge separation, electronic excitation and electron density transition in a molecule. The HOMO-LUMO electron counterplots of dyes **1a-1c, 2a-2c** and **3a-3c** were calculated using B3LYP/6-311++G(d,p) and are shown in Figure S1. The charge transfer (CT) performance in dyes is well understood by the overlap of atomic orbitals involved in the electronic transitions, i.e. mainly from HOMO to LUMO which is associated with a change in dipole moment. From the HOMO-LUMO plots, electron densities in HOMO and LUMO are equally populated in dyes containing no substituents at 7 positions (**1a**, **2a**, **3a**) which indicate that there is no efficient CT character in this cases. On the other hand, the electron density is spread all over the molecule and density migrates to LUMO when the molecules are functionalized with donor groups, -OCH_3 and -$N(CH_2CH_3)_2$. The results indicate that there is an efficient intramolecular charge transfer (ICT) and charge separation in this cases. Therefore, the facility of CT in dyes **1a-1c, 2a-2c** and **3a-3c** increases in the sequences of donors, -H < -OCH_3 < -$N(CH_2CH_3)_2$. From the above observations, it is evident that in the donor substituted molecules the energy of HOMO increases while the energy of LUMO decreases leading to red shifted absorption as well as emission. It can be concluded that the dye **3c** having a strong donor, -$N(CH_2CH_3)_2$ and strong acceptor NO_2 possess efficient CT character.

3.4b *Natural charges and natural bond orbital (NBO) analysis from Fock Matrix*: Natural charges in the ground state, as well as excited state, enabled to understand the intramolecular charge distribution and interactions. The natural charges on selected atoms within the dyes **1c**, **2c** and **3c** have been shown in Table 3 and similarly, for remaining dyes (**1a**, **1b**, **2a**, **2b**, **3a**, and

Table 3. Natural charges on selected atoms of dyes **1c**, **2c** and **3c** in acetonitrile medium.

Atom No	1c	Atom No	2c	Atom No	3c
N18	0.00411	N31	0.00592	N30	0.00642
C9	0.00541	C11	0.00645	C11	0.00639
C17	−0.00463	C27	0.00039	C27	0.00464
O11	−0.00175	O13	−0.00100	N47	−0.02849
C1	−0.01116	C1	−0.00575	O45	−0.01162
C10	−0.00287	O14	−0.00304	O46	−0.01159

Table 4. Selected second-order perturbation energies E(2) (Donor→Acceptor π interactions) of dye **3c** in acetonitrile medium.

Donor(i)	Type	ED[a](e)	Acceptor (j)	Type	ED[a](e)	E(2)[b] [kJ/mol]	E(j) - E(i)[c] [a.u.]	F(i, j)[d] [a.u.]
N30	LP(1)	1.68951	C4 - C5	π*	0.01723	24870.71	1.4	5.71
			C5 - C15	π*	0.02244	1375.25	7.37	3.071
			C7 - C11	π*	0.01989	173.86	9.02	1.153
			C18 - C20	π*	0.02502	27.17	8.3	0.458
			C23 - C27	π*	0.02237	1481.16	8.31	3.385
			C27 - N47	π*	0.10153	10370.98	3.39	5.591
			O45 - N47	π*	0.055	922.24	9.89	2.887
			O46 - N47	π*	0.05471	2300.14	7.22	3.975
C 4 - C 5	π	1.97419	C7 - C11	π*	0.01989	76.27	0.04	0.053
C15 - C18	π	1.97473	C23 - C27	π*	0.02237	29287.67	0.04	0.983
			O45 - N47	π*	0.055	594.93	1.62	0.902
C27 - N47	π	1.98861	C7 - C11	π*	0.01989	833	0.09	0.275
			C15 - C18	π*	0.01447	34.59	0.98	0.164
			O45 - N47	π*	0.055	616.48	0.96	0.693
O45 - N47	π	1.99575	O45 - N47	π*	0.055	201.3	2.68	1.115

Where, [a] ED is the electron density, [b] E(2) means energy of hyperconjugative interactions (stabilization energy), [c] Energy difference between donor and acceptor i and j NBO orbitals, [d] F(i, j) is the Fock matrix element between i and j NBO orbitals.

3b) are shown in Table S5. It is as expected and found that the donor fragment carries a positive charge while acceptor fragment has a negative charge. The positive natural charge on N-atom indicates that the moiety carrying N-atom is an effective electron donor unit while the one having the negative value represents the good electron acceptor unit. The dyes **1c**, **2c** and **3c** show more NBO charges on the electron donor group as compared to the other dyes hence the dyes **1c**, **2c** and **3c** exhibit strong electron transfer towards acceptor. The second order Fock matrix analysis has been constructed to investigate the donor-acceptor interactions and stability of the coumarin dyes using B3LYP/6-311++G(d,p) level of theory, in order to comprehend the intramolecular charge transfer and delocalization of electron density. Higher the E(2) value more the intensive molecular interaction between the electron donor and electron acceptor leading to a greater extent of conjugation in the system. These interactions are observed as an increase the electron density on C=C bond to the antibonding orbitals of the C=C bond. Table 4 shows that there exists intramolecular hyperconjugative interaction between donor and acceptor for **3c**. Similarly, for the other dyes, the values have been listed in Table S6. Strong intramolecular hyper conjugative interaction of the π electrons of C=C to the C=C* bond orbital of the conjugated system leads to stabilization of the molecule. It has been observed that the hyperconjugative interaction of π electrons of N_1 (LP) with the π* of the C_4-C_5 bond increases the electron density by 0.01723 leading to the stabilization energy of ∼ 24870.71 kJ/mol. The nitrogen of N, N-diethylamino group, N_1 (LP) is also conjugated with the C5-C15, C7-C11, C18-C20, C23-C27, C27-N47, O45-N47 and O46-N47 with their stabilization energies 1375.25, 173.86, 27.17, 1481.16, 10370.98, 922.24 and 2300.24 kJ/mol. respectively. In

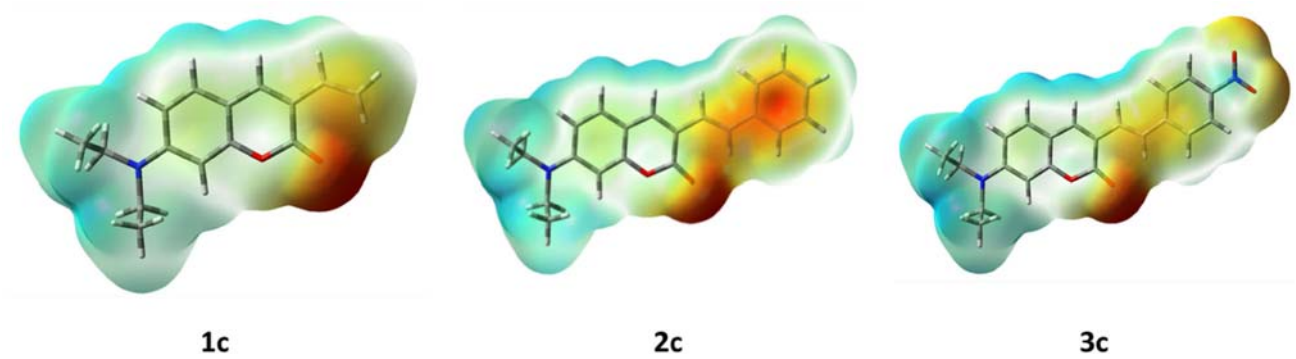

Figure 5. MEP surface plots of coumarin dyes **1c**, **2c** and **3c**.

this regard, the most energetic interaction of $C_{15} - C_{18}$ conjugates with π* of C23 - C27 and O45 - N47 of 29287.67 and 594.93 kJ/mol. Also, the planarity of the nitro group with the donor group and phenyl ring increases the conjugation between them which signifies the electron delocalization from the donor to the acceptor. These intramolecular interactions within the π to π* are responsible for the CT from donor to acceptor end leads to polarization and optical nonlinearity within the molecule.

3.4c *Molecular electrostatic potential (MEP) analysis*: MEP analysis is an important tool in describing the reactivity of molecules. It gives information on shape, size, charge density, polarity, and site of chemical reactivity of molecules. The 3D MEP plots of **1c**, **2c** and **3c** are constructed from B3LYP/6- 311++G(d,p) optimized geometry with the help of visualization program, Gauss View 5.0 and shown in Figure 5. MEP values of **1c**, **2c** and **3c** are ±0.101, ±0.00957 and ±0.00894 a.u. respectively. MEP plot shows that negative potential site (electrophilic region) is located over carbonyl group as well as a double bond in **1c** and the positive potential sites (nucleophilic regions) are found around the hydrogen atoms. In case of **2c**, a negative potential is located over the carbonyl group along with π-bridge and phenyl ring. But in case of **3c**, the electron density is located on carbonyl group, π-bridge and nitro group.

3.4d *Triplet state populations and electrophilicity index*: The triplet state of a molecule has a lower energy compared to the singlet state. The TD-DFT computation showed that there are three triplet states between S_0 and S_1 states in **1a** and **1b**, while there were only two such triplet states in **2a**, **2b**, **2c**, **3a** and **3b**. However, there was only one triplet state lying between S_0 and S_1 in **1c** and **3c**. The energy intersystem crossing, ΔE_{ISC} which is the energy difference between S_1 and the triplet state closer to S_1, was calculated in each case and shown in Table S7 along with the quantum yield values. It turns out that substitutions on 7 and 3 positions directly influence the fluorescence quantum yield of coumarin dyes. The fluorescence quantum yield of **3c** is lower (< 0.01) as compared to the other dyes, which is in the good agreement with the lower ΔE_{ISC} values. When there are no donor and acceptor groups as in **1a**, **2a** and **3a** the ΔE_{ISC} values are higher which leads to an increase in quantum yield. The ΔE_{ISC} values in each series are in the order **1a** > **1b** > **1c**, **2a** > **2b** > **2c** and **3a** > **3b** > **3c**.

The chemical stability of a dye depends on its hardness and softness. From the HOMO – LUMO energy band gap, one can find whether the molecule is hard or soft.[72,73] The dyes having the high energy band gap lead to more hardness and vice versa. The hardness of a dye is inversely proportional to the electrophilicity index (ω) (Table S7). The ω can be defined as an electrophilic power of the molecule which signifies the energy lowering associated with the maximum electron flow between donor and acceptor orbitals. From the Table S7, it is seen that the energy band gap (E_L-E_H) of the dyes are in good agreement with ω and the trend is **1a** > **1c, 2a** > **2c** and **3a** < **3c**. The hardness of a molecule can be determined by the formula,

$$\eta = \frac{(-\varepsilon HOMO + \varepsilon LUMO)}{2} \tag{7}$$

Where, η = hardness of molecule, ε HOMO and ε LUMO are the energies of the HOMO and LUMO orbitals respectively.

3.5 *Polarizability and hyperpolarizability*

The total polarizability (α_0), polarizability anisotropy ($\Delta\alpha$) and the static first order hyperpolarizability (β_0) were calculated using global hybrid (GH) and range separated hybrid (RSH) functionals with 6-311++G(d,p) basis set as implemented in Gaussian 09. The results of α_0, $\Delta\alpha$, β_0 and mean absolute error (MAE) of each dye

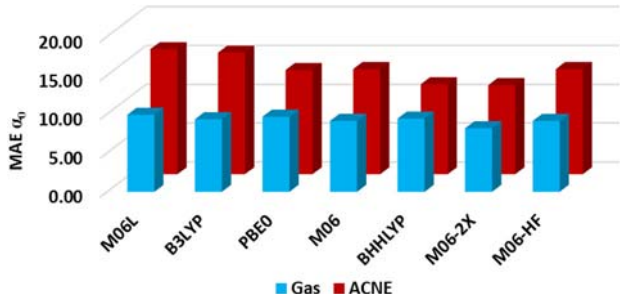

Figure 6. Polarizability ($\alpha_0 \times 10^{-24}$ e.s.u.) mean absolute error (MAE) in the gas phase and solvent acetonitrile (ACNE) obtained from global hybrid functions (GHs).

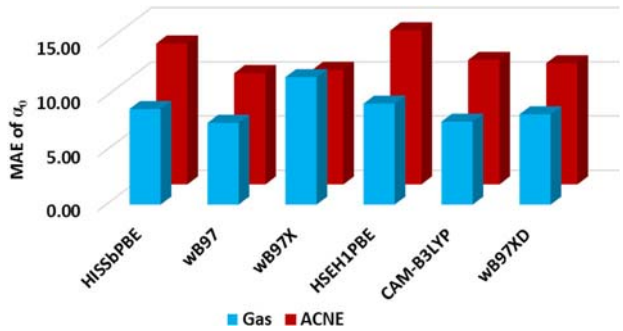

Figure 7. Mean absolute error (MAE) of polarizability ($\alpha_0 \times 10^{-24}$ e.s.u.) in the gas phase and solvent acetonitrile (ACNE) obtained from range separated hybrid functionals (RSHs).

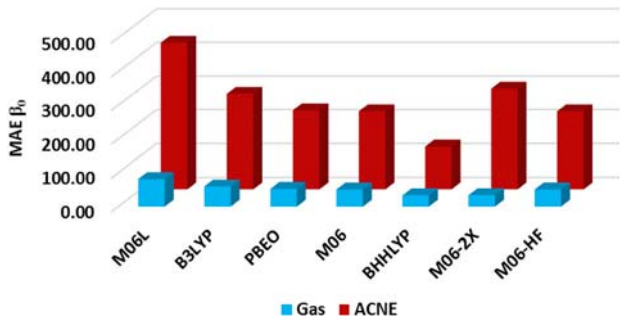

Figure 8. Hyperpolarizability ($\beta_0 \times 10^{-30}$ e.s.u.) mean absolute error (MAE) in the gas phase and solvent acetonitrile (ACNE) by global hybrid functions (GHs).

in every case are calculated in the gas phase, as well as the inclusion of solvent (acetonitrile), are shown in Table S8, S9, S10, S11, S12, and S13. The comparative results of MAE with respect to each functional are shown in Figures 6, 7, 8 and 9.

It is clearly observed that the **1a**, **1b**, **1c** dyes show enhanced α_0, $\Delta\alpha$, and β_0 with the substitution pattern as -H <-OCH_3 < -$N(CH_2CH_3)_2$ group. A similar trend was observed for styryl dyes **2a**, **2b** and **2c** where one of the H in the terminal carbon of the vinyl is replaced by phenyl, as well as in **3a**, **3b** and **3c** where phenyl ring

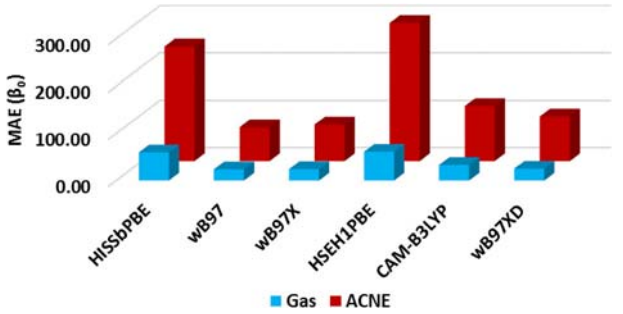

Figure 9. Hyperpolarizability ($\beta_0 \times 10^{-30}$ e.s.u.) mean absolute error (MAE) in the gas phase and solvent acetonitrile (ACNE) by range separated hybrid functions (RSHs).

carries a nitro group para to the vinyl group. The dye **3c** containing both NO_2 and diethylamino group exhibited the largest hyperpolarizability in all the functionals used for comparison. This outcome signifies that the substitution pattern of donor and acceptor directly affects the magnitudes of α_0 and β_0. In order to assess the cause of enhanced β_0 value, we have correlated it with the dipole moment (Figure S2, S3 and S4). All the dyes show a linear increase in dipole moment with increasing β_0 value which may be due to donor and acceptor group lying on the same axis (along with the direction of dipole moment) as revealed by the optimized geometry in the ground and excited state (Figure 5). These results show noticeable enhancement of CT characteristic in the studied dyes.

The GHs and RSHs give large errors in computing the polarizability (α_0) and hyperpolarizability values (β_0) of the coumarin dyes under investigation. The positive values of mean absolute error (MAE) signifies that they tend to overestimate α_0 and β_0 values. The trends in MAE in various functionals are shown in Figures 6, 7, 8, 9. The values of α_0 obtained using from the global hybrid functionals - M06-2X, BHHLYP, M06, and PBE0 - are comparable (Figure 6). This observation is not surprising because the HF % exchange for the hybrid BHHLYP, M06-2X, PBE0, and M06 functionals are respectively 54, 50, 27 and 25.[54] Among the RSHs comparable values were obtained with the pairs of wB97 - wB97X, and CAM-B3LYP - wB97XD show more comparable precise values of α_0 as compared to GHs (Figure 7). The results of β_0 are displayed in Table S12 and S13. The values of β_0 obtained from the GHs M06, M06HF, and PBE0 are found to be comparable with each other (Figure 8). The B3LYP functional underestimates the values of β_0. The trend among the GHs is found to be BHHLYP < M06-2X < M06 < M06HF < PBE0 < B3LYP < M06-L. As for the RSHs concerned, CAM-B3LYP and wB97-XD gave comparable β_0 values and much closer to each other. The functionals HISSbPBE

Table 5. Diagonal electronic and vibrational contributions to dipole polarizabilities and first hyperpolarizabilities of dyes **1a**-**1c**, **2a**-**2c** and **3a**-**3c** obtained from of B3LYP/6-311++G(d,p) level in acetonitrile medium. (All values are in a.u.).

Property	1a	1b	1c	2a	2b	2c	3a	3b	3c
α^{e}_{xx}	327.3	395.8	516.1	595.5	662.89	835.8	733.7	847.31	1124.1
α^{e}_{yy}	−13.5	21.6	−25.3	−48.4	48.5	−47.5	56.8	53.3	−50.1
α^{e}_{zz}	159.4	174.4	231.0	258.5	277.1	322.3	284.6	300.0	344.4
α^{v}_{xx}	21.1	60.0	85.1	23.9	67.3	104.0	78.1	148.3	248.5
α^{v}_{yy}	7.5	10.3	15.1	14.0	18.3	26.6	21.9	25.0	27.1
α^{v}_{zz}	22.5	35.7	76.8	102.2	133.5	179.4	215.3	133.9	123.4
α^{e}	157.7	197.2	240.6	268.5	329.5	370.2	358.4	400.2	472.8
α^{v}	17.0	35.3	59.0	46.7	73.1	103.3	105.1	102.4	133.0
α^{v}/α^{e}	9.3	5.6	4.1	5.7	4.5	3.6	3.4	0.3	3.6
$\alpha^{e}+\alpha^{v}$	174.7	232.6	299.6	315.2	402.6	473.5	463.5	502.6	605.8
β^{e}_{xx}	657.0	−3027.1	−10013.4	7393.9	−1436.5	−17812.9	25553.9	−49616.8	−113147.3
β^{e}_{yy}	−462.8	1178.7	−1990.4	−1085.7	1780.0	−2729.5	−2468.7	2784.0	−113147.3
β^{e}_{zz}	31.1	181.4	581.2	204.3	569.4	979.3	−773.0	1259.4	1854.8
β^{v}_{xx}	382.6	1638.7	3025.8	−156.8	2231.7	5862.7	−8641.0	16689.3	34918.1
β^{v}_{yy}	−46.8	43.8	−37.0	−203.3	105.7	−89.1	100.9	−70.8	24.6
β^{v}_{zz}	0.0	0.0	233.9	0.2	−0.5	592.2	−0.1	1.3	−74.9
β^{e}	75.1	−555.7	−3807.5	2170.8	304.3	−6521.0	7437.4	−15191.1	−74813.2
β^{v}	111.9	560.8	1074.2	−120.0	779.0	2121.9	−2846.7	5539.9	11622.6
β^{v}/β^{e}	0.7	−1.0	−3.5	−18.1	0.4	−3.1	−2.6	−0.4	−6.4
$\beta^{e}+\beta^{v}$	187.0	5.1	−2733.3	2050.9	1083.3	−4399.1	4590.6	−9651.2	−63190.6

and HSEH1PBE overestimate the $\beta_0$values as compared to the other RSHs. The functionals wB97 and wB97-X behave exactly similar manner (Figure 9). The reason for this behavior is attributed to the fact that as against RSHs, GHs do not have HF % exchange in the long-range. This comparison of functionals suggests that the global hybrid functionals might be overestimating the hyperpolarizability results. Also, the polarizability and hyperpolarizability values were considerably lower in the absence of solvent environment. The computed values of α_0 and β_0 of the coumarins investigated here are several times greater than that of urea.[74]

3.6 *Vibrational contribution to the linear and NLO response*

Vibrational anharmonicity originates from the coupling between the electronic and nuclear motions. In other words coupling between the electronic polarization and vibrational motions leads to a considerable vibrational contribution to the NLO response. DFT is an effective computational tool to study the vibrational contribution towards polarizability and hyperpolarizability of NLO materials. The vibrational contributions to static electronic polarizabilities and hyperpolarizabilities were calculated using B3LYP/6-311++G(d,p) in acetonitrile medium. The vibrational contribution to each element of α and β tensor has been estimated and compared with the corresponding electronic counterpart and tabulated in Table 5. The results show that the power of an individual component indicates a significant delocalization of charges in the particular direction. It is noticed that the largest value of hyperpolarizability component is of β_{xx} and subsequently delocalization of electron cloud is more in the x-direction (3c = 34918.1). The ratios of vibrational to electronic contribution for polarizability (a^v/a^e) are 9.3, 5.6, 4.1, 5.7, 4.5, 3.6, 3.4, 0.3, 3.6 whereas for hyperpolarizability (β^v/β^e) are 0.7, -1.0, -3.5, -18.1, 0.4, -3.1, -2.6, -0.4, -6.4 for 1a-3c respectively. The computed vibrational hyperpolarizability (β^v) are found to be of the same order as electronic one (β^e). The results confirm that the vibrational motions play a fundamental role in determining the NLO properties of these dyes.

3.7 *The correlation of BLA and BOA with NLO parameters*

BLA and BOA are the geometric and electronic parameters which depend on the length of π-conjugation, the strength of the donor-acceptor group and the surrounding media. The BLA and BOA values of S_0 and S_1 geometries were calculated from the optimized geometries of S_0 and S_1 state. The BLA and BOA parameters at S_0 and S_1 state for all the dyes are correlated with β_0 values in Figures 10 and f11 and the results of BLA and

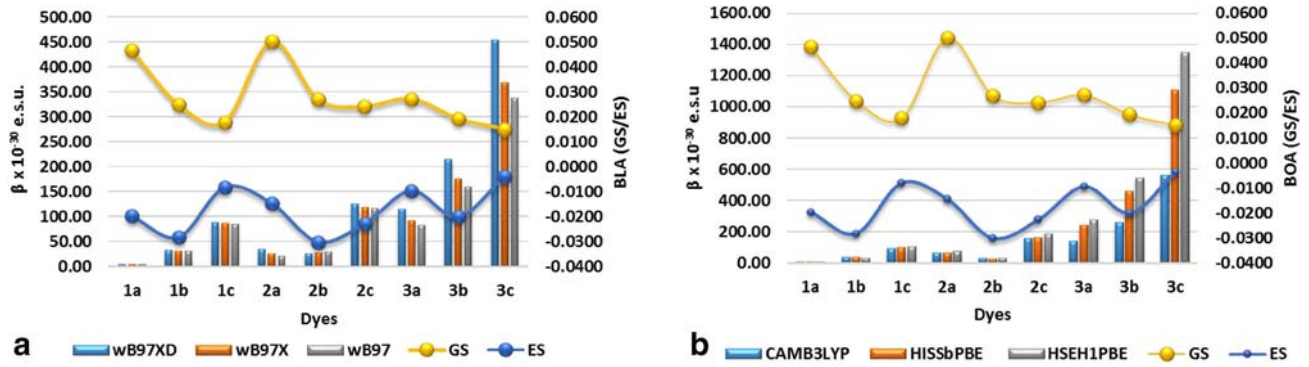

Figure 10. (**a**, **b**). BLA at ground state and excited state (GS/ES) vs. hyperpolarizability (by RSH functionals) of dyes **1a**-**1c**, **2a**-**2c** and **3a**-**3c**.

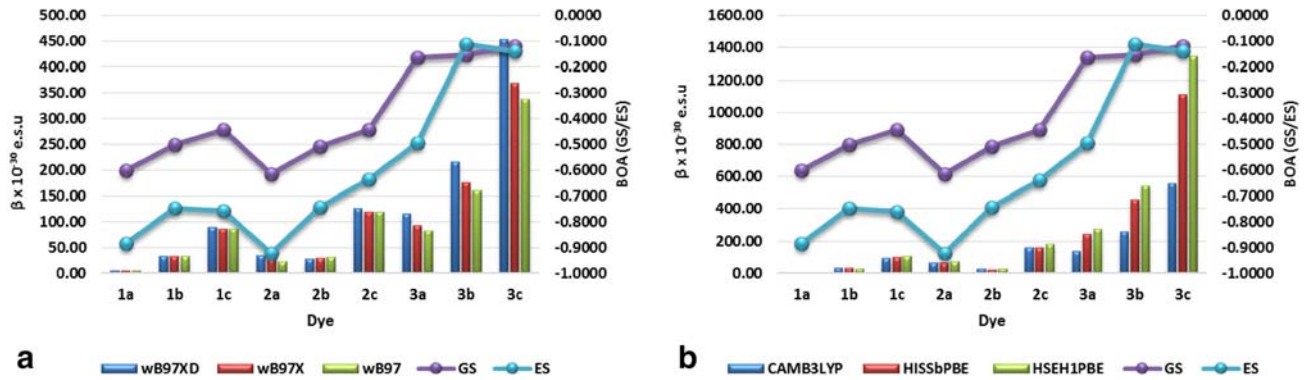

Figure 11. (**a**, **b**). BOA at ground state and excited state (GS/ES) vs. hyperpolarizability (by RSH functionals) of dyes **1a**-**1c**, **2a**-**2c** and **3a**-**3c**.

BOA are shown in Table 1. The Figures 10 and 11 show that there is a linear correlation of β_0 values with BLA and BOA values in S_0 and S_1 state respectively. From Table S1 it is seen that the BLA values decrease in the order **1a** > **1b** > **1c** in the ground state whereas for BOA the trend is found to be the reverse. A similar trend is seen for **2a**–**2c** and **3a**–**3c**. Moreover, in the excited state, no such regular trend is found and the values of BLA and BOA tend to zero suggesting a high degree of polarization. Greater the polarization more are the μ, α_0 and β_0 values which lead to a decrease in BLA and BOA (Figures 10, 11). Furthermore, the magnitudes of μ, α_0 and β_0 increase with increasing donor-acceptor strength and increasing π-conjugation length, especially in case of **3c**. The trends in μ, α_0 and β_0 values are in good agreement with the trends in BLA and BOA values (Figures S2, S3 and S4).

4. Conclusions

In summary, linear and nonlinear optical properties of styryl and vinyl coumarin dyes have been extensively studied by means of DFT and TD-DFT using global hybrid (GH) and range separated hybrid (RSH) functionals using 6-311++G(d,p) basis set. The GHs overestimated α_0 and β_0 values. The RSH functionals CAM-B3LYP, wB97, wB97-X and wB97-XD gave comparable α_0 and β_0 values and the values are good agreement with each other. An increase in the donor strength in the sequence -H < -OCH_3 < -$N(CH_2CH_3)_2$ enhanced charge transfer characteristics and increased NLO response in the coumarin dyes. Lowering HOMO – LUMO energy band gap brings about an increase in μ, α_0, and β_0. The β_0 value of coumarin dyes reaches the maximum as the bond length alternation (BLA) and bond order alternation (BOA) parameters tend to zero. Ratio of vibrational contribution with electronic contribution of polarizability (α^v/α^e) and first hyperpolarizability ($\bar{\beta}^v/\bar{\beta}^e$) decreased in the order -H < -OCH_3 < -$N(CH_2CH_3)_2$. High electrophilicity index suggested good photostability of the molecules. The singlet triplet energy gap analysis is found to be in good agreement with the trends in quantum yield. These coumarin dyes are proved to be the better performing NLOphores than standard urea. The coumarin dyes studied here are good candidates for the materials in nonlinear optics considering their higher static first order hyperpolarizability (β_0).

Supplementary Information (SI)

This supplementary information includes HOMO LUMO diagram, plots of dipole moment against polarizability, hyperpolarizability, geometrical parameters, natural charges, components of polarizability and hyperpolarizability obtained from different functionals. Supplementary Information is available at www.ias.ac.in/chemsci.

Acknowledgements

Kiran Avhad and Amol Jadhav are thankful to University Grant Commission, New Delhi, India for providing research fellowship.

References

1. Dalton L R, Sullivan P A and Bale D H 2010 Electric field poled organic electro-optic materials: State of the art and future prospects *Chem. Rev.* **110** 25
2. Chang C, Chen C, Chou, C, Kuo W and Jeng R 2005 Polymers for electro-optical modulation *J. Macromol. Sci., Polym. Rev.* **45** 125
3. Gieseking R L, Mukhopadhyay S, Risko C, Marder S R and Brédas J L 2014 25th Anniversary article: Design of polymethine dyes for all-optical switching applications—guidance from theoretical and computational studies *Adv. Mater.* **26** 68
4. Coe B J, Foxon S P, Harper E C, Helliwell M, Raftery J, Swanson C A, Brunschwig B S, Clays K, Franz E, Garin J, Orduna J, Horton P N and Hursthouse M B 2010 Evolution of linear absorption and nonlinear optical properties in V-shaped Ruthenium(II)-based chromophores *J. Am. Chem. Soc.* **132** 1706
5. Wu J, Wilson B A, Smith Jr D W and Nielsen S O 2014 Towards an understanding of structure-nonlinearity relationships in triarylamine-based push-pull electro-optic chromophores: The influence of substituent and molecular conformation on molecular hyperpolarizabilities *J. Mater. Chem. C* **2** 2591
6. Yang Y, Xu H, Liu F, Wang H, Deng G, Si P, Huang H, Bo S, Liu J, Qiu L, Zhen Z and Liu X 2014 Synthesis and optical nonlinear property of Y-type chromophores based on double-donor structures with excellent electro-optic activity *J. Mater. Chem. C* **2** 5124
7. Kutuvantavida Y, Williams G V M, Bhuiyan M D H, Raymond S G and Kay A J 2015 Effects of chromophore conjugation length and concentration on the photostability of indoline-based nonlinear optical chromophore/polymer films *J. Phys. Chem. C* **119** 3273
8. Gheorma I L and Gopalakrishnan G K 2007 Flat frequency comb generation with an integrated dual-parallel modulator *IEEE Photonics Technol. Lett.* **19** 1011
9. Liu J, Gao W, Kityk I V, Liu X and Zhen Z 2015 Optimization of polycyclic electron-donors based on julolidinyl structure in push-pull chromophores for second order NLO effects *Dyes Pigments* **122** 74
10. Gryl M, Kozieł M, Stadnicka K, Matulková I, Němec I, Tesařová N and Němec P 2013 Lidocaine barbiturate: A promising material for second harmonic generation *CrystEngComm* **15** 3275
11. Tathe A B and Sekar N 2016 Red emitting NLOphoric 3-styryl coumarins: Experimental and computational studies *Opt. Mater. (Amst).* **51** 121
12. Derkowska B, Mulatier J C, Fuks I, Sahraoui B, Phu X N and Andraud C 2001 Third-order optical nonlinearities in new octupolar molecules and their dipolar subunits *J. Opt. Soc. Am. B* **18** 610
13. Papagiannouli I, Iliopoulos K, Gindre D, Sahraoui B, Krupka O, Smokal V, Kolendo A and Couris S 2012 Third-order nonlinear optical response of push-pull azobenzene polymers *Chem. Phys. Lett.* **554** 107
14. Sahraoui B, Luc J, Meghea A, Czaplicki R, Fillaut J L and Migalska-Zalas A 2009 Nonlinear optics and surface relief gratings in alkynyl–ruthenium complexes *J. Opt. A Pure Appl. Opt.* **11** 24005
15. Lin T C, Cole J M, Higginbotham A P, Edwards A J, Piltz R O, Perez-Moreno J, Seo J Y, Lee S C, Clays K and Kwon O P 2013 Molecular origins of the high-performance nonlinear optical susceptibility in a phenolic polyene chromophore: Electron density distributions, hydrogen bonding, and ab initio calculations *J. Phys. Chem. C* **117** 9416
16. Tathe A B and Sekar N 2016 NLOphoric red emitting bis coumarins with O-BF2-O core-synthesis, photophysical properties and DFT studies *J. Fluoresc.* **26** 471
17. Abraham E, Oberlé J, Jonusauskas G, Lapouyade R and Rullière C 1997 Photophysics of 4-dimethylamino 4′-cyanostilbene and model compounds: Dual excited states revealed by sub-picosecond transient absorption and kerr ellipsometry *Chem. Phys.* **214** 409
18. Grabowski Z R, Rotkiewicz K and Rettig W 2003 Structural changes accompanying intramolecular electron transfer: Focus on twisted intramolecular charge-transfer states and structures *Chem. Rev.* **103** 3899
19. Pines D, Pines E and Rettig W 2003 Dual fluorescence and excited-state structural relaxations in donor-acceptor stilbenes *J. Phys. Chem. A* **107** 236
20. Singh A K, Darshi M and Kanvah S 2000 α,ω-diphenylpolyenes cabable of exhibiting twisted intramolecular charge transfer fluorescence: A fluorescence and fluorescence probe study of nitro- and nitrocyano-substituted 1,4-diphenylbutadienes *J. Phys. Chem. A* **104** 464
21. Carlotti B, Flamini R, Kikaš I, Mazzucato U and Spalletti A 2012 Intramolecular charge transfer, solvatochromism and hyperpolarizability of compounds bearing ethenylene or ethynylene bridges *Chem. Phys.* **407** 9
22. Li C, Li M, Li Y, Zhang Y, Cai Z, Shi Z, Wang X, Zhang D and Cui Z 2016 Improved poling efficiency of polyurethanes containing spindle-like chromophores by a functional group tuning for nonlinear optic (NLO) materials *RSC Adv.* **6** 18178
23. Li M, Huang S, Zhou X H, Zang Y, Wu J, Cui Z, Luo J and Jen A K Y 2015 Poling efficiency enhancement of tethered binary nonlinear optical chromophores for achieving an ultrahigh $N^3 R_{33}$ figure-of-merit of 2601 Pm V^{-1} *J. Mater. Chem. C* **3** 6737
24. Kim T D, Kang J W, Luo J, Jang S H, Ka J W, Tucker N, Benedict J B, Dalton L R, Gray T, Overney R M, Park D H, Herman W N and Jen A K Y 2007 Ultralarge and

thermally stable electro-optic activities from supramolecular self-assembled molecular glasses *J. Am. Chem. Soc.* **129** 488
25. Zhang X, Li M, Shi Z, Wan Y, Zhao L, Jin R, Wang X, Zhang D, Yi M and Cui Z 2011 Design, synthesis, and characterization of crosslinkable doped NLO materials based on polyurethanes containing spindle-type chromophores *Macromol. Chem. Phys.* **212** 879
26. Cheng Y J, Luo J, Huang S, Zhou X, Shi Z, Kim T D, Bale D H, Takahashi S, Yick A, Polishak B M, Jang S H, Dalton L R, Reid P J, Steier W H and Jen A K Y 2008 Donor-acceptor thiolated polyenic chromophores exhibiting large optical nonlinearity and excellent photostability *Chem. Mater.* **20** 5047
27. Moeckli P 1980 Preparation of some new red fluorescent 4-cyanocoumarin dyes *Dyes Pigments* **1** 3
28. Griffiths J, Millar V and Bahra G S 1995 The influence of chain length and electron acceptor residues in 3-substituted 7-N,N-diethylaminocoumarin dyes *Dyes Pigments* **28** 327
29. Lanke S K and Sekar N 2016 Aggregation induced emissive carbazole-based push pull NLOphores: Synthesis, photophysical properties and DFT studies *Dyes Pigments* **124** 82
30. Lanke S K and Sekar N 2015 Rigid coumarins: A complete DFT, TD-DFT and non linear optical property study *J. Fluoresc.* **25** 1469
31. Lindasay 1973 United States Patent 191, No. 1984
32. Moylan C R 1994 Molecular hyperpolarizabilities of coumarin dyes *J. Phys. Chem.* **98** 13513
33. Moerner W E and Silence S M 1994 Polymeric photorefractive materials *Chem. Rev.* **94** 127
34. Tathe A B, Gupta V D and Sekar N 2015 Synthesis and combined experimental and computational investigations on spectroscopic and photophysical properties of red emitting 3-styryl coumarins *Dyes Pigments* **119** 49
35. Huang S T, Jian J L, Peng H Z, Wang K L, Lin C M, Huang C H and Yang T C K 2010 The synthesis and optical characterization of novel iminocoumarin derivatives *Dyes Pigments* **86** 6
36. Tathe A B and Sekar 2016 N Red-emitting NLOphoric carbazole-coumarin hybrids-synthesis, photophysical properties and DFT studies *Dyes Pigments* **129** 174
37. Lanke S K and Sekar 2015 N Rigid coumarins: A complete DFT, TD-DFT and non linear optical property study *J. Fluoresc.* **25** 1469
38. Brédas J L 1985 Relationship between band gap and bond length alternation in organic conjugated polymers *J. Chem. Phys.* **82** 3808
39. Roncali J 2007 Molecular engineering of the band gap of π-conjugated systems: Facing technological applications *Macromol. Rapid Comm.* **28** 1761
40. Mullekom H A M van, Vekemans J A J M, Havinga and Meijer E W 2001 Developments in the chemistry and band gap engineering of donor–acceptor substituted conjugated polymers *Mat. Sci. Eng. R* **32** 1
41. Marder S R, Gorman C B, Tiemann B G and Cheng L T 1993 Stronger acceptors can diminish nonlinear optical response in simple donor-acceptor polyenes *J. Am. Chem. Soc.* **115** 3006
42. Bouit P A, Aronica C, Toupet L, Guennic B Le, Andraud C and Maury O 2010 Continuous symmetry breaking induced by ion pairing effect in heptamethine cyanine dyes: Beyond the cyanine limit *J. Am. Chem. Soc.* **132** 4328
43. Meyers F, Marder S R, Pierce B M and Bredas J L 1994 Electric field modulated nonlinear optical properties of donor-acceptor polyenes: Sum-over-states investigation of the relationship between molecular polarizabilities (alpha, beta, and gamma) and bond length alternation *J. Am. Chem. Soc.* **116** 10703
44. Kwon O P, Kwon S J, Jazbinsek M, Seo J Y, Kim J T, Seo J I, Lee Y S, Yun H and Gunter P 2011 Phenolic polyene crystals with tailored physical properties and very large nonlinear optical response *Chem. Mater.* **23** 239
45. Kohn W and Sham L J 1965 Self-consistent equations including exchange and correlation effects *Phys. Rev.* **140** 1133
46. Frisch M J, Trucks G W, Schlegel H B, Scuseria G E, Robb M A, Cheeseman J R, Scalmani G, Barone V, Mennucci B, Petersson G A, Nakatsuji H, Caricato M, Li X, Hratchian H P, Izmaylov A F, Bloino J, Zheng G, Sonnenberg J L, Hada M, Ehara M, Toyota K, Fukuda R, Hasegawa J, Ishida M, Nakajima T, Honda Y, Kitao O, Nakai H, Vreven T, Montgomery Jr J A, Peralta J E, Ogliaro F, Bearpark M, Heyd J J, Brothers E, Kudin K N, Staroverov V N, Keith T, Kobayashi R, Normand J, Raghavachari K, Rendell A, Burant J C, Iyengar S S, Tomasi J, Cossi M, Rega N, Millam J M, Klene M, Knox J E, Cross J B, Bakken V, Adamo C, Jaramillo J, Gomperts R, Stratmann R E, Yazyev O, Austin A J, Cammi R, Pomelli C, Ochterski J W, Martin R L, Morokuma K, Zakrzewski V G, Voth G A, Salvador P, Dannenberg J J, Dapprich S, Daniels A D, Farkas O, Foreman J B, Ortiz J V, Cioslowski J and Fox D J 2010 G. 09; Revision C.01, Gaussian, Inc., Wallingford, CT
47. Lee C, Yang W and Parr R G 1988 Development of the Colle-Salvetti correlation-energy formula into a functional of the electron density *Phys. Rev. B* **37** 785
48. Becke A D 1993 Density-functional thermochemistry. III. The role of exact exchange *J. Chem. Phys.* **98** 5648
49. Stephens P J, Devlin F J, Chabalowski C F and Frisch M J 1994 Ab initio calculation of vibrational absorption and circular dichroism spectra using density functional force fields *J. Phys. Chem.* **98** 11623
50. Petersson G A, Bennett A, Tensfeldt T G, Al-Laham M A, Shirley W A and Mantzaris J A 1988 Complete basis set model chemistry. I. The total energies of closed-shell atoms and hydrides of the first-row elements *J. Chem. Phys.* **89** 2193
51. Runge E and Gross E K U 1984 Density-functional theory for time-dependent systems *Phys. Rev. Lett.* **52** 997
52. Tomasi J, Mennucci B and Cammi R 2005 Quantum mechanical continuum Solvation models *Chem. Rev.* **105** 2999
53. Vidya S, Ravikumar C, Hubert Joe I, Kumaradhas P, Devipriya B and Raju K 2011 Vibrational spectra and structural studies of nonlinear optical crystal ammonium D, L-tartrate: A density functional theoretical approach *J. Raman Spectrosc.* **42** 676
54. Howard J C, Enyard J D and Tschumper G S 2015 Assessing the accuracy of some popular DFT methods for computing harmonic vibrational frequencies of water clusters *J. Chem. Phys.* **143** 214103

55. Henderson T M, Izmaylov A F, Scuseria G E and Savin A 2008 Assessment of a Middle-Range Hybrid Functional *J. Chem. Theory Comput.* **4** 1254
56. Peverati R and Truhlar D G 2014 Quest for a universal density functional: The accuracy of density functionals across a broad spectrum of databases in chemistry and physics *Philos. T. Roy. Soc. A* **372** 20120476
57. Laurent A D and Jacquemin D 2013 TD-DFT benchmarks: A review *Int. J. Quantum Chem.* **113** 2019
58. Caricato M, Trucks G W, Frisch M J and Wiberg K B 2010 Electronic transition energies: A study of the performance of a large range of single reference density functional and wave function methods on valence and rydberg states compared to experiment *J. Chem. Theory Comput.* **6** 370
59. Marom N, Tkatchenko A, Rossi M, Gobre V V, Hod O, Scheffler M and Kronik L 2011 Dispersion interactions with density-functional theory: Benchmarking semiempirical and interatomic pairwise corrected density functionals *J. Chem. Theory Comput.* **7** 3944
60. Bhattacharya D, Shil S, Misra A, Bytautas L and Klein D J 2015 Photomagnetic and nonlinear optical properties in cis-trans green fluoroprotein chromophore coupled bisimino nitroxide diradicals *Int. J. Quantum Chem.* **115** 1561
61. Nénon S, Champagne B and Spassova M I 2014 Assessing long-range corrected functionals with physically-adjusted range-separated parameters for calculating the polarizability and the second hyperpolarizability of polydiacetylene and polybutatriene chains *Phys. Chem. Chem. Phys.* **16** 7083
62. Eriksson E S and Eriksson L A 2011 Predictive power of long-range corrected functionals on the spectroscopic properties of tetrapyrrole derivatives for photodynamic therapy *Phys. Chem. Chem. Phys.* **13** 7207
63. Benassi E 2017 Benchmarking of density functionals for a soft but accurate prediction and assignment of 1 H and 13 C NMR chemical shifts in organic and biological molecules *J. Comput. Chem.* **38** 87
64. Zhao Y and Truhlar D G 2011 Density functional theory for reaction energies: Test of meta and hybrid meta functionals, range-separated functionals, and other high-performance functionals *J. Chem. Theory Comput.* **7** 669
65. Gerber I C and Ángyán J G 2005 Hybrid functional with separated range *Chem. Phys. Lett.* **415** 100
66. Salzner U and Aydin A 2011 Improved prediction of properties of π-conjugated oligomers with range-separated hybrid density functionals *J. Chem. Theory Comput.* **7** 2568
67. Baer R, Livshits E and Salzner U 2010 Tuned range-separated hybrids in density functional theory *Annu. Rev. Phys. Chem.* **61** 85
68. Refaely-Abramson S, Baer R and Kronik L 2011 Fundamental and excitation gaps in molecules of relevance for organic photovoltaics from an optimally tuned range-separated hybrid functional *Phys. Rev. B* **84** 75144
69. Meganathan C, Sebastian S, Kurt M, Lee K W and Sundaraganesan N 2010 Molecular structure, spectroscopic (FTIR, FTIR gas phase, FT-raman) first-order hyperpolarizability and HOMO-LUMO analysis of 4-methoxy-2-methyl benzoic acid *J. Raman Spectrosc.* **41** 1369
70. Fu Y, Shen W and Li M 2008 Geometries and electronic structures of co-oligomers and co-polymers based on tricyclic nonclassical thiophene: A theoretical study *Macromol. Theor. Simul.* **17** 385
71. Gordo J, Avó J, Parola A J, Lima J C, Pereira A and Branco P S 2011 Convenient synthesis of 3-vinyl and 3-styryl coumarins Org. Lett. 13 5112.
72. Mahalakshmi G and Balachandran V 2015 NBO, HOMO, LUMO Analysis and vibrational spectra (FTIR and FT raman) of 1-amino 4-methylpiperazine using ab initio HF and DFT methods *Spectrochim. Acta Part A* **135** 321
73. Geerlings P, De Proft F and Langenaeker W 2003 Conceptual density functional theory *Chem. Rev.* **103** 1793
74. Arivazhagan M, Kavitha R and Subhasini V P 2014 Conformational analysis, UV–VIS, MESP, NLO and NMR studies of 6-methoxy-1,2,3,4-tetrahydronaphthalene *Spectrochim. Acta Part A* **128** 701